JOURNAL OF MATERIALS SCIENCE 21 (1986) 2014–2026

Toughening of polyester resins through blending with polyolefins

D. L. WILFONG, A. HILTNER, E. BAER
Department of Macromolecular Science, Case Western Reserve University, Cleveland, Ohio 44106, USA

The effect of blending low concentrations (1 to 10%) of polyolefins on the crystallization and irreversible deformation behaviour of polyester (PET) resins was investigated. The olefin particles did not nucleate crystallization of PET from the melt but did depress the rate of crystallization. Decreases in the cold crystallization temperature of PET during heating from the glassy state in blends with linear low density polyethylene (LLDPE) and high density polyethylene (HDPE) were attributed to stress induced crystallization created by large volume expansions associated with melting of the olefin particles. A sharp transition in fracture strain for PET and the PET–olefin blends was observed with strain rate, where at low strain rates fracture occurred during work hardening, and as the strain rate increased, fracture occurred during cold drawing. The transition corresponded with a decrease in draw stress, a decrease in draw ratio and an increase in density of the neck. A shift in the transition to higher strain rates for the blend compositions was attributed to increased rates of crystallization and orientation due to strain induced crystallization at the stress fields surrounding the olefin particles. As the strain rate increased and the cold drawing process became more adiabatic, the mechanical behaviour was controlled by the kinetics of crystallization and orientation.

1. Introduction

The enhancement of toughness in polymers is widely achieved commercially by blending. Polystyrene (PS) is impact modified through the incorporation of rubber particles which act both to initiate crazes and to terminate them before they develop into catastrophic cracks [1–3]. This crazing process in high impact polystyrene (HIPS) can be controlled through particle size and distribution [4, 5]. Toughening by induced crazing in HIPS is maximized with rubber particles of approximately 2 to 5 μm in diameter [6, 7].

In polypropylene (PP) and poly(acrylonitrile-butadiene-styrene) (ABS) the size of the modifying rubber particles determines the mode of toughening [8–10]. It is generally accepted that induced crazing is the major energy absorption mechanism for both PP and ABS when rubber particles larger than 1 μm in diameter are incorporated. However, PP and ABS containing rubber particles 0.1 to 0.5 μm in diameter exhibit a slight propensity for crazing. In this case, the toughening mechanism involves cavitation of the small rubber particles which subsequently promotes localized shear deformation. This mechanism of particle voiding and shear deformation is responsible for the enhanced energy absorption in poly(vinyl chloride) modified with methacrylate-butadiene-styrene, ABS or chlorinated polyethylene particles less than 1 μm in diameter [11–13].

The impact modification mechanism for rubber toughened nylon is generally considered to involve energy dissipation by both crazing and shear yielding of the matrix [14]. Nylon toughened with polyethylene-g-maleic anhydride particles approximately 0.3 μm in diameter deforms primarily by shear flow induced by stress concentrations surrounding the particles [15]. Crazing and particle matrix debonding are also thought to contribute to the energy absorption mechanism. Polycarbonate is toughened by incorporation of polyethylene particles which, unlike the rubber modified systems, do not adhere well to the matrix [16, 17]. Impact modification is attributed to shear stress concentrations at the olefin particles which promote plastic flow and particle–matrix debonding.

Fracture toughness of polyester (PET) resins is improved with the addition of glass spheres ranging from 1 to 100 μm in diameter [18, 19]. It is suggested that the enhanced fracture toughness results from a combination of crack pinning by the particles and increased plastic deformation of the matrix at the pinned crack [20]. The predominant factor influencing toughness is thought to be the distance between particles rather than sphere size. Toughness is maximized when there is poor adhesion between the PET matrix and the glass beads [18–20]. This is attributed to increased plastic deformation resulting from higher stress concentrations when a void is created.

In this study, the crystallization and irreversible deformation behaviour of crystallizable polyester resins blended with low concentrations (1 to 10%) of linear low density polyethylene (LLDPE), high density polyethylene (HDPE), polypropylene (PP) of poly(4-methylpentene-1) (TPX) particles was

0022–2461/86 $03.00 + .12

investigated. The effect of the olefin particles on the nucleation, rate of crystallization and strain rate dependent toughening of PET was evaluated.

2. Experimental procedures

2.1. Materials

The polymers used in this study were polyethylene terephthalate (PET), Cleartuf 1006, Cleartuf 7207 and Vituf 1001A with intrinsic viscosities of 1.04, 0.72 and 1.04, respectively, (Goodyear Tyre and Rubber Co., Akron, Ohio), LLDPE (Dowlex 2045; 0.920 g cm^{-3}), HDPE (Dowlex 7065; 0.965 g cm^{-3}) (Dow Chemical Co., Midland, Michigan), PP (Hercules SA861; 0.900 g cm^{-3}) (Hercules, Philadelphia, Pennsylvania), and TPX (Mitsui RT-18; 0.833 g cm^{-3}) (Mitsui, Tokyo, Japan). Blends of Cleartuf 1006 PET with 3% by weight LLDPE, HDPE, PP and TPX were prepared through melt extrusion from a Sterling Transfermix Extruder with an L : D ratio of 42 : 1 into 30 mil thick sheets by Goodyear. Vituf 1001A PET with 1, 3 and 5% and Cleartuf 7207 PET with 1, 3, 5 and 10% by weight LLDPE were prepared through melt extrusion from a Prodex Extruder with an L : D ratio of 24 : 1 into 40 mil thick sheets at 302 to 307 and 274 to 279° C, respectively, by Goodyear.

2.2. Scanning electron microscopy

Blend morphologies were determined by examining scanning electron micrographs of surfaces from cryogenically fractured samples. Specimens were prepared by bending either strips (10 mm × 150 mm) of the sheet material or the necked portion of the deformed tensile specimen to fracture immediately after they were immersed in liquid nitrogen for 5 min. The fractured surfaces were sputter coated with gold before observation in the Joel scanning electron microscope (SEM) Model 35 CF.

2.3. Thermal analysis

Ten mg specimens of Cleartuf 1006 PET and the PET 3% olefin blends were heated at 20° C min^{-1} in a Perkin-Elmer DSC II Differential Scanning Calorimeter (DSC) to 310° C and held at this temperature for 5 min before cooling at rates of 2.5 to 40° C min^{-1}. Specimens quench cooled to 30° C at 320° C min^{-1} in the DSC following 5 min at 310° C were subsequently heated at rates of 5 to 80° C min^{-1}. DSC samples were cut from the necked regions of tensile specimens which were strained to fracture and the heat of fusion determined after heating at 20° C min^{-1}. Indium and tin were used as standards for temperature and enthalpy calibration. All materials were dried in a vacuum oven at 100° C for 24 h before examination.

2.4. Hotstage optical microscopy

The spherulitic structure of Cleartuf 1006 PET was examined under an aus Jena optical microscope in the cross-polarized transmission mode. Specimens of PET and a PET–3% LLDPE blend were prepared by melting approximately 3 mg of polymer on an optical microscope slide with a Mettler FP 52 hotstage at 310° C for 5 min. The thin molten film was then cooled on the hotstage at controlled rates of 2.5 and 5° C min^{-1} from 310 to 80° C. Prior to any melt processing steps, all materials were dried in a vacuum oven at 100° C for 24 h.

2.5. Mechanical behaviour

Tensile specimens were cut from the extruded sheet in accordance with the ASTM D-1708-66 geometry. Stress and strain measurements based on the initial cross-sectional area of the tensile specimen and crosshead displacement were conducted on both a standard Instron and a material testing machine (MTS). Strain rates of 10 to 500% min^{-1} were utilized with the Instron and 500 to 57 000% min^{-1} with the MTS. Stress and strain measurements for the Vituf 1001A PET–LLDPE and Cleartuf 7207 PET–LLDPE samples were performed only at the strain rates utilized with the MTS. At least six samples were tested at each strain rate for all compositions and the results averaged.

2.6. Infrared thermometry

The temperature rise during the cold drawing process was measured both directly and non-invasively. This was done with an Everest Interscience Microscopic Infrared Thermometer Model 2300 (Everest, Tustin, California) which measures the temperature of a 1 mm target spot at a distance of 10 cm with a response time of 0.03 sec and a resolution of 0.5° C. The infrared thermometer was focused on the tensile specimen and the subsequent temperatures recorded during tensile deformation. The peak temperature was recorded when the propagating neck front passed through the target spot. Two to four measurements were made at each strain rate for each composition.

2.7. Density

The density of deformed and undeformed specimens was measured with a pycnometer and aqueous solutions of either NaBr or methanol. Deformed samples were prepared by straining tensile specimens to fracture at strain rates of 500 to 57 000% min^{-1}. Samples for analysis were cut from the necked region of the tensile specimen at a site away from the fractured ends. At least two measurements were made at each strain rate for each composition.

3. Results

3.1. Cleartuf 1006 PET blended with LLDPE, HDPE, PP and TPX

3.1.1. Morphology

SEM micrographs of the freeze fractured surfaces of the PET blends are shown in Fig. 1. The morphology consisted of spherical olefin particles distributed throughout a PET matrix. The particle size distribution was determined by measuring at least sixty particle diameters for each composition, Fig. 2. For LLDPE, HDPE or PP in PET, the distribution is narrow with average sphere diameters in the range of 0.3 to 1.1 μm. The TPX particles show a very broad size distribution with particles up to 5 μm.

3.1.2. Crystallization from the melt

A typical DSC cooling thermogram for PET–HDPE

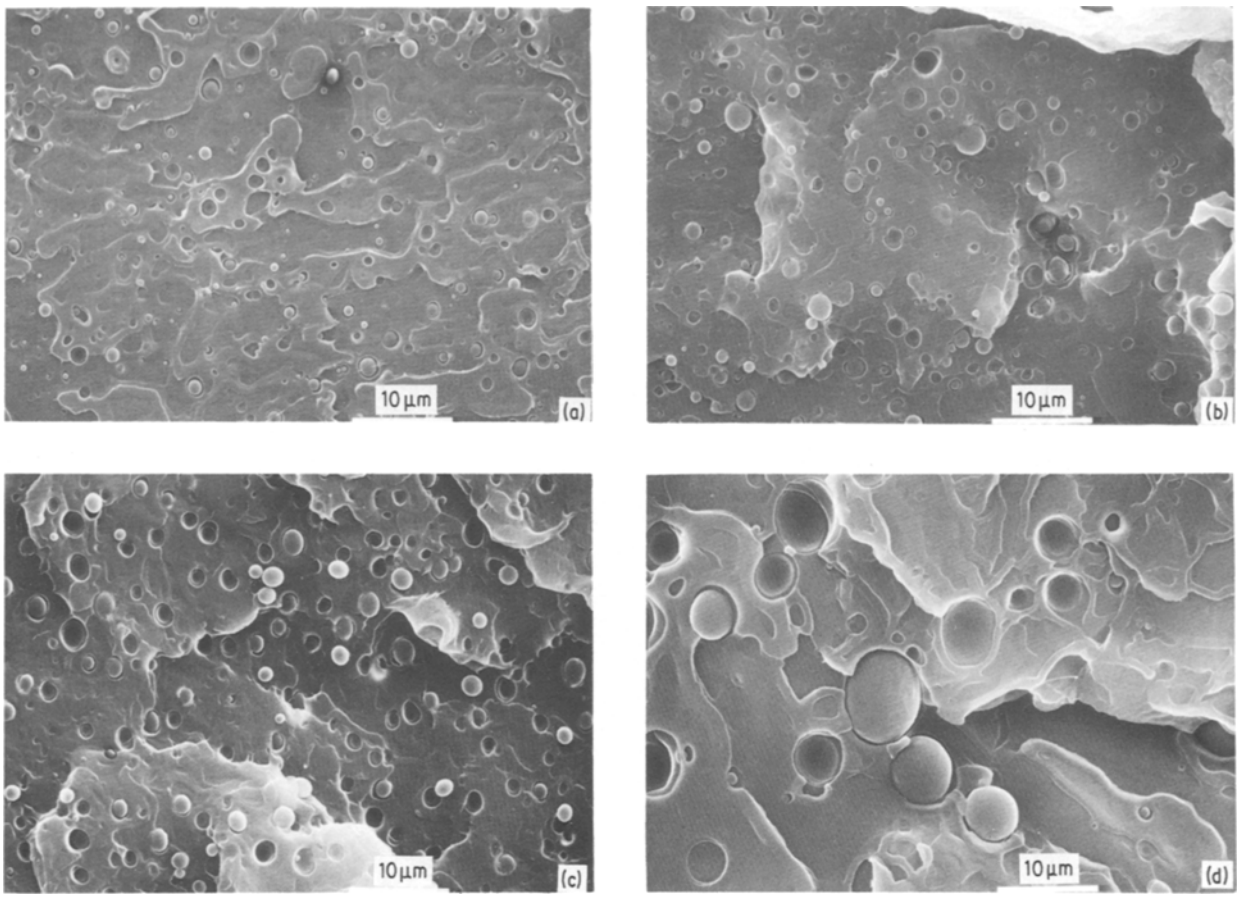

Figure 1 SEM micrographs of the freeze fractured surfaces of Cleartuf 1006 PET blended with 3% by weight (a) LLDPE, (b) HDPE, (c) PP and (d) TPX.

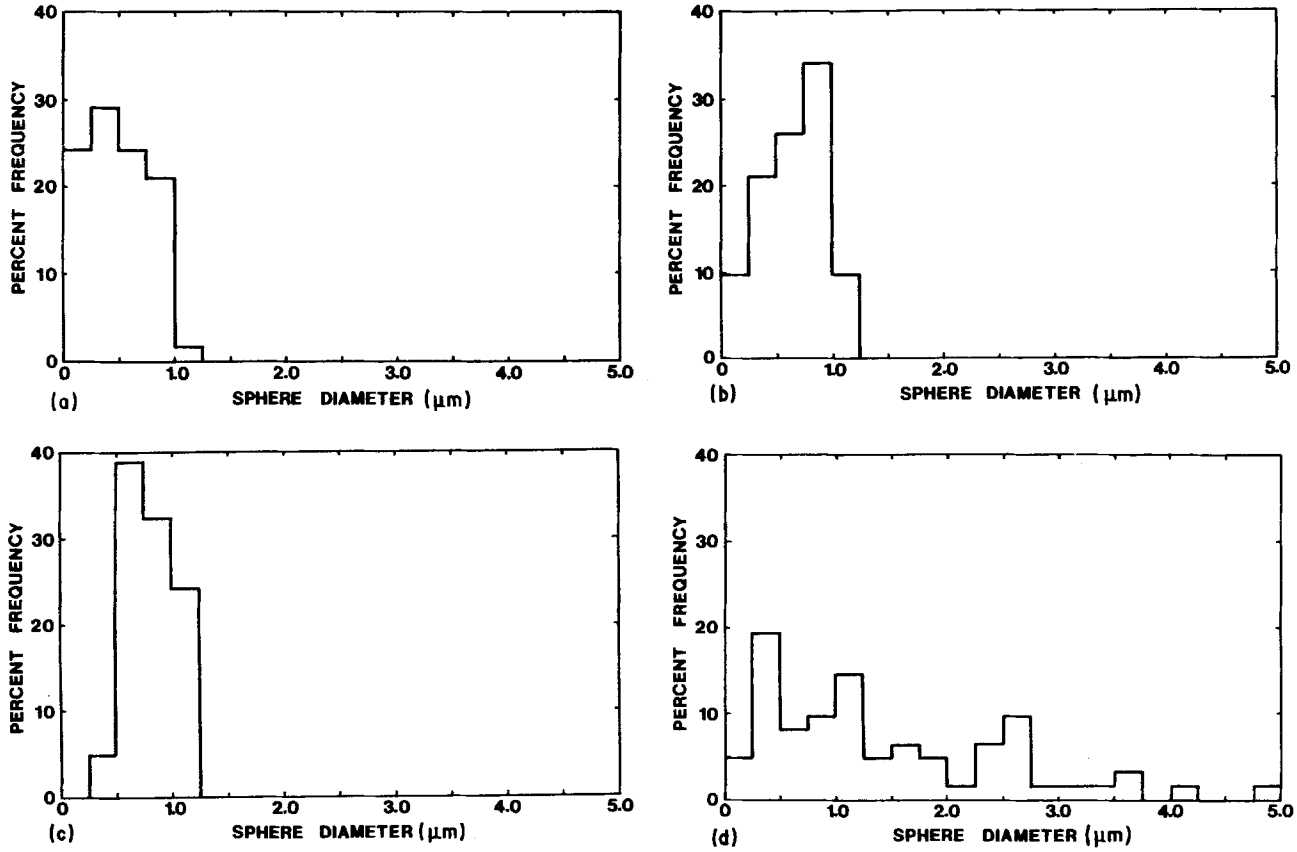

Figure 2 Particle size distribution determined from SEM micrographs of the Cleartuf 1006 PET blend freeze fractured surfaces. At least 60 particle diameters were measured for each composition. (a) PET–LLDPE, $\bar{x} = 0.6 \pm 0.3\,\mu m$, (b) PET–HDPE, $\bar{x} = 0.7 \pm 0.3\,\mu m$, (c) PET–PP, $\bar{x} = 0.9 \pm 0.2\,\mu m$, (d) PET–TPX, $\bar{x} = 1.5 \pm 1.1\,\mu m$.

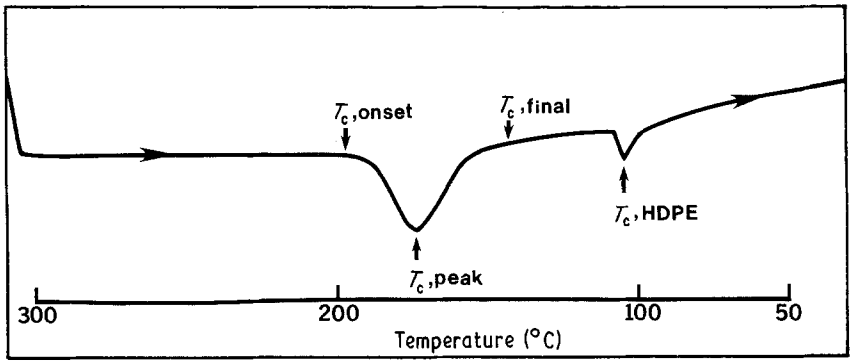

Figure 3 A typical cooling thermogram for PET–HDPE cooled at 10° C min^{-1} from 310 to 30° C.

is shown in Fig. 3. Cooling from 310° C first resulted in crystallization of PET followed by crystallization of the olefin. This behaviour was typical for PET and the PET–olefin blends for cooling rates of 2.5 to 20° C min^{-1}. However, crystallization of the TPX component in PET–TPX blends was not detected at any cooling rate. The crystallization onset temperature measured for the PET component in the blends was within 5° C of that determined for the homopolymer and decreased in a linear manner with increasing cooling rate.

The heat of crystallization of PET, Fig. 4, was independent of both composition and cooling rate for cooling rates from 2.5 to 20° C min^{-1}. The drop in crystallization heat for all the compositions at a cooling rate of 40° C min^{-1} was indicative of incomplete crystallization, although unmodified PET crystallized to a greater extent than PET in the blends.

The crystallization exotherm in the cooling thermograms was broader in the blend compositions than for the homopolymer at all cooling rates. An increase in the crystallization time is indicative of a broadening of the crystallite or spherulite size distribution. Optical micrographs of the PET spherulites grown from the homopolymer and PET–LLDPE blend melts at two cooling rates are shown in Figs 5a to d. The spherulite size was 2.5 to 3 times greater and the spherulite size distribution broader for the blend than for the homopolymer.

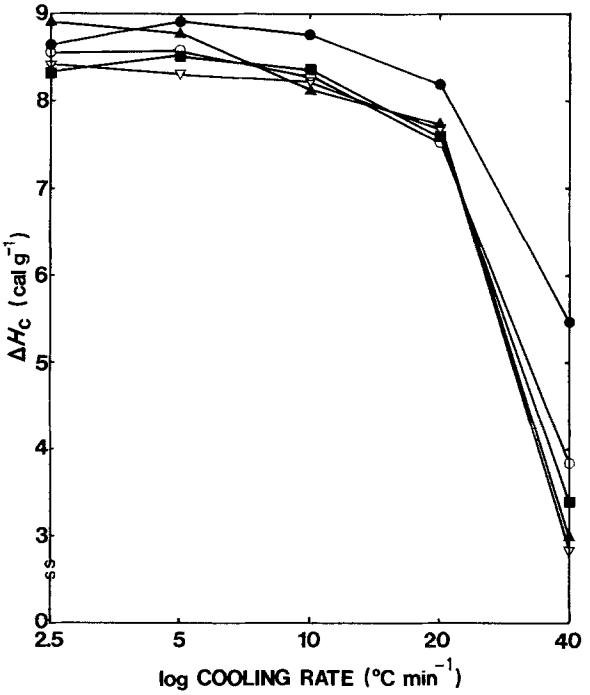

Figure 4 The heats of crystallization as a function of cooling rate determined for Cleartuf 1006 PET and the blend compositions, ● PET, ■ PET–LLDPE, ▲ PET–HDPE, ▽ PET–PP, ○ PET–TPX. (1 cal = 4.18 J).

3.1.3. Crystallization from the glassy state

Heating thermograms for melt quenched specimens are shown in Fig. 6. Heating from the glass revealed the glass transition temperature, T_g, of PET, melting of the olefin in the PET– LLDPE and PET–HDPE blends at 123 and 132° C, respectively, followed by cold crystallization of PET. The melting endotherm for LLDPE is not observed in Fig. 6 due to the small sample size utilized but is clearly seen with much larger DSC specimens. A decrease in the PET cold crystallization temperature of 4 to 9° C for PET–LLDPE and 1 to 5° C for PET–HDPE blends was observed, but there was no significant change in the cold crystallization temperatures for PET–PP and PET–TPX blends. No significant differences in the heats of cold crystallization between PET and the PET–olefin blends were observed.

3.1.4. Irreversible deformation behaviour

The first observable irreversible deformation event for the drawn tensile specimens was the formation of a single shear band which developed into a sharp neck. A typical stress–strain curve for PET and the blends is shown schematically in Fig. 7. The yield point was observed at about 6 to 7% elongation and corresponded with the formation of the sharp neck. Propagation of the stable neck was reflected in the cold drawn portion of the stress–strain curve. After the neck had spread through the entire gauge length of the tensile specimen, work hardening and uniform extension of the neck was observed.

The neck formed in PET had a translucent appearance at all strain rates except 6000% min^{-1} where regions of the neck were white and opaque. However, the necked material of the blends was white and opaque at all strain rates.

In Fig. 8, the average yield stress is plotted against strain rate. The yield stress of PET was only slightly higher than the blends. As typically observed for polymers, the yield stress increased linearly with strain rate.

The average draw stress for PET and the blends is shown in Fig. 9. All the compositions exhibited an

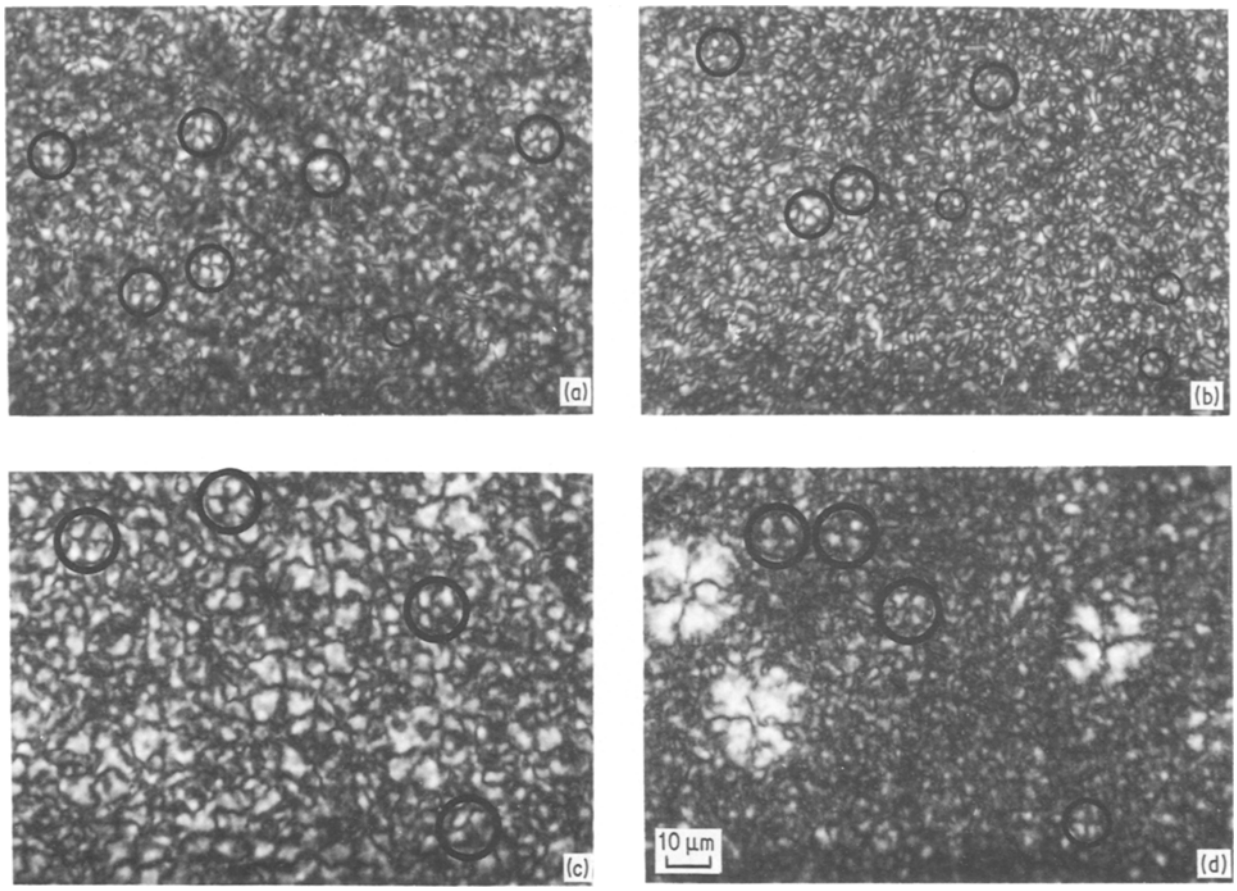

Figure 5 Optical micrographs of the spherulitic crystallization of (a) Cleartuf 1006 PET cooled from the melt at 2° C min^{-1}, (b) 5° C min^{-1}, (c) PET–LLDPE cooled from the melt at 2° C min^{-1}, (d) 5° C min^{-1}.

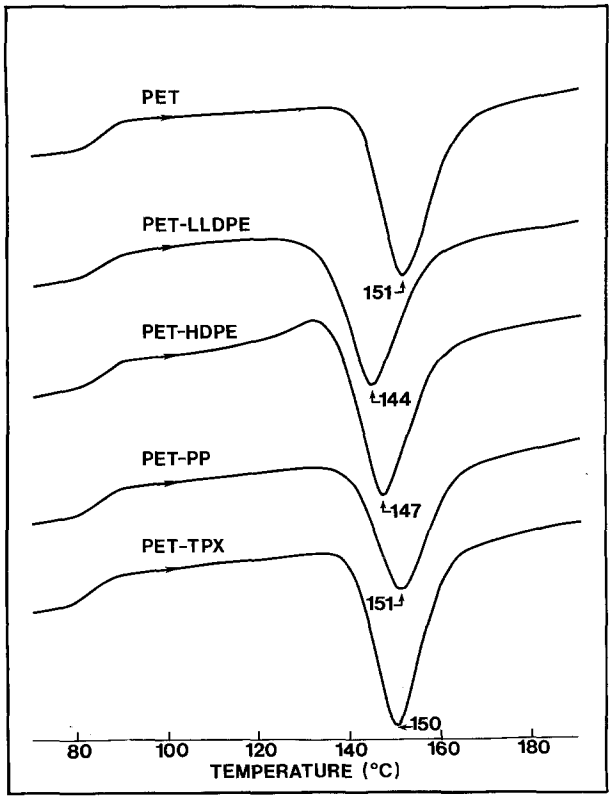

Figure 6 Heating thermograms for Cleartuf 1006 and the blend compositions recorded at a heating rate of 40° C min^{-1}.

increase in draw stress between strain rates of 500 and 6000% min^{-1}. However, at 6000% min^{-1} the draw stress for PET declined significantly. The draw stress of the other blends increased with strain rate; the highest draw stress was exhibited by PET–LLDPE at 57 000% min^{-1}.

The draw ratio for PET and the blends is shown in Fig. 10 as a function of strain rate. All compositions displayed an increase in draw ratio with strain rate from 10 to 6000% min^{-1}. At 10 000% min^{-1} the draw ratio of PET dropped dramatically while the draw ratio of the blends levelled off. The blends exhibited a decrease in draw ratio at 57 000% min^{-1}; the decrease was in the order of PET–TPX > PET–PP > PET–HDPE > PET–LLDPE.

At low strain rates, specimens fractured during the work hardening process. As the strain rate increased, a transition in fracture strain was observed with fracture occurring during the cold drawing process. In Fig. 11, the circled points denote fracture during cold drawing. The strain at fracture increased with strain rate up to 6000% min^{-1}. A drop in fracture strain by an order of magnitude was observed for PET as the strain rate increased from 6000 to 10 000% min^{-1}. The drop in fracture strain accompanied the transition from fracture during work hardening to fracture during cold drawing. The blends exhibited only a 4 to 8%

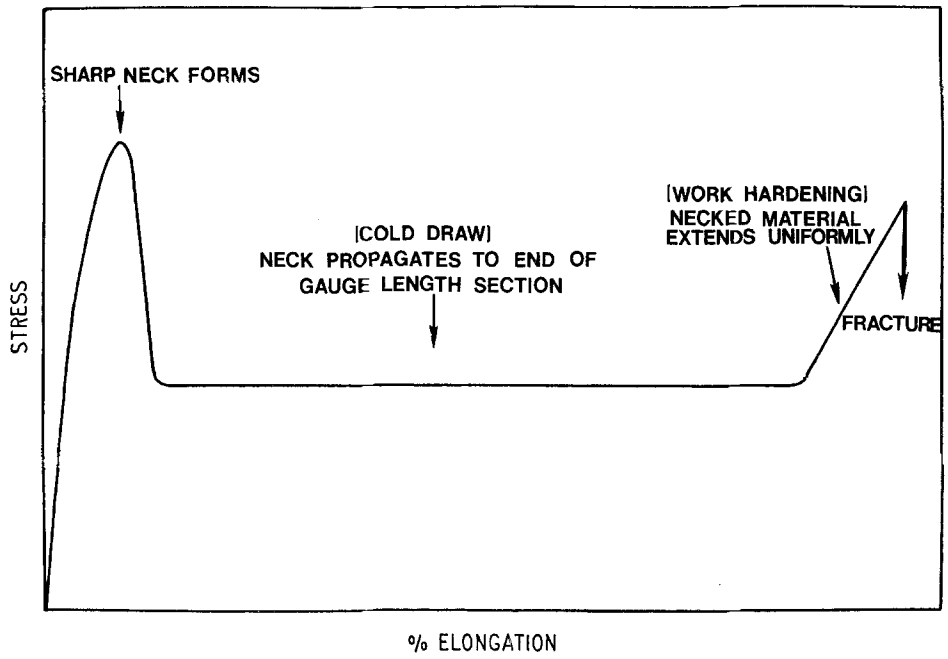

Figure 7 A schematic representation of a typical stress–strain curve for PET and the blend compositions.

decrease in fracture strain at 10 000% min^{-1}, but a further increase in strain rate for the blends with LLDPE, HDPE, PP and TPX resulted in 42, 47, 64 and 85% decreases in fracture strain, respectively. The transition in fracture behaviour coincided with the previously noted decreases in draw stress and draw ratio.

An increase in temperature of the necked region of a tensile specimen during cold drawing was observed. The peak temperature, T_p, was measured at the interface of the propagating neck and the unnecked material. A plot of T_p and the difference between T_p and the ambient temperature, T_a, is shown in Fig. 12. T_p increased with strain rate. At the highest strain rates, the T_p for PET levelled at approximately the T_g of PET. The values of T_p for the PET–olefin blends (92 to 123° C) were significantly greater than for the PET (79° C) at the highest strain rates.

Tensile specimens exhibited strain induced crystallization during deformation. Heats of fusion for specimens strained to fracture at 100 and 10 000% min^{-1} were approximately 35 and 43 J g^{-1}, respectively, and independent of composition. The amount of strain induced crystallinity was 22 to 34% higher than the crystallinity produced by cold crystallization.

3.1.5. Density

The densities of deformed and undeformed specimens of PET, PET–LLDPE and PET–TPX as a function of strain rate are shown in Fig. 13. The density of PET

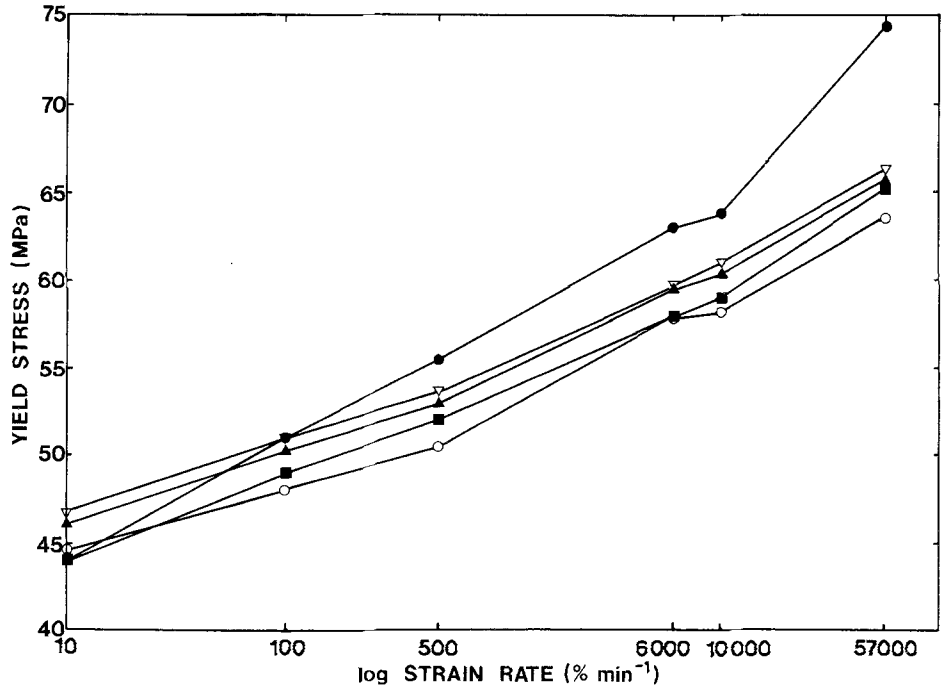

Figure 8 Average yield stress against strain rate for Cleartuf 1006 PET and the blend compositions, ● PET, ■ PET–LLDPE, ▲ PET–HDPE, ▽ PET–PP, ○ PET–TPX.

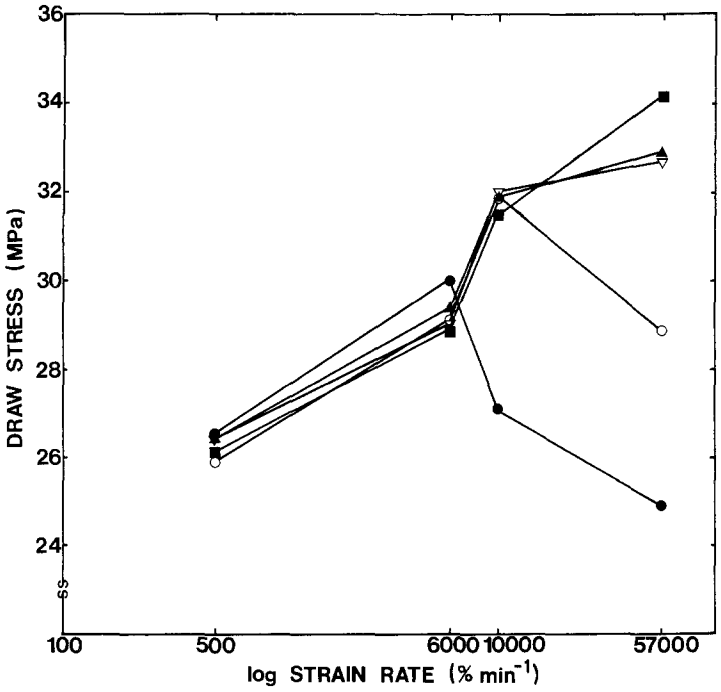

Figure 9 The average draw stress as a function of strain rate for Cleartuf 1006 PET and the PET–olefin blends, ● PET, ■ PET–LLDPE, ▲ PET–HDPE, ▽ PET–PP, ○ PET–TPX.

and the PET–TPX blend went through a minimum at strain rates of 6000 and 10 000% min^{-1}, respectively. Only a gradual decrease in density with no minimum was exhibited by the PET–LLDPE blends. The increase in density for PET and the PET–TPX blend corresponded with the transition in fracture strain, draw stress and draw ratio.

An SEM micrograph of the freeze fractured surface of the necked portion of PET–TPX drawn to fracture is shown in Fig. 14. Large voids surrounding the olefin particles were observed for specimens fractured at strain rates of 500 to 10 000% min^{-1}. No voiding was observed at a strain rate of 57 000% min^{-1} when fracture occurred during cold drawing.

3.2. Vituf 1001A and Cleartuf 7207 PET blended with 1 to 10% LLDPE

3.2.1. Morphology

Micrographs of freeze fractured surfaces of Cleartuf 7207 PET with 1, 3, 5 and 10% LLDPE are shown in Fig. 15. Similar particle sizes and distributions were observed for both Vituf 1001 PET and Cleartuf 7207 PET blended with LLDPE. As the per cent LLDPE in the PET increased, the average sphere diameter became larger, the distribution broadened. The distribution varied from approximately 0.1 to 1.1 μm at 1% LLDPE, 0.2 to 1.8 μm at 3% LLDPE, 0.5 to 2.9 μm at 5% LLDPE, to 1.1 to 4.1 μm at 10% LLDPE.

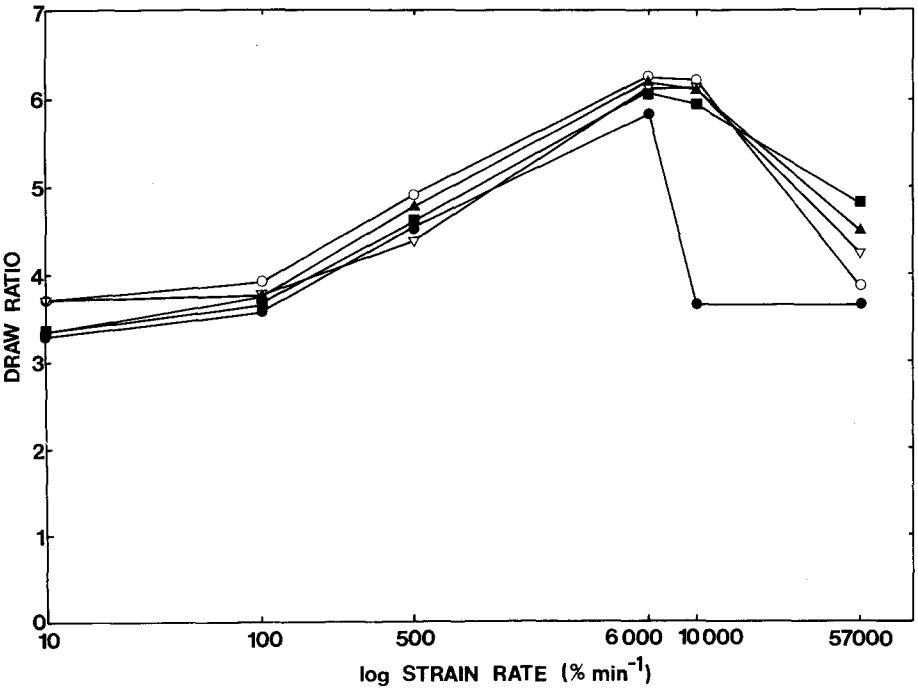

Figure 10 Average draw ratios evaluated as a function of strain rate for Cleartuf 1006 PET and the blend compositions, ● PET, ■ PET–LLDPE, ▲ PET–HDPE, ▽ PET–PP, ○ PET–TPX.

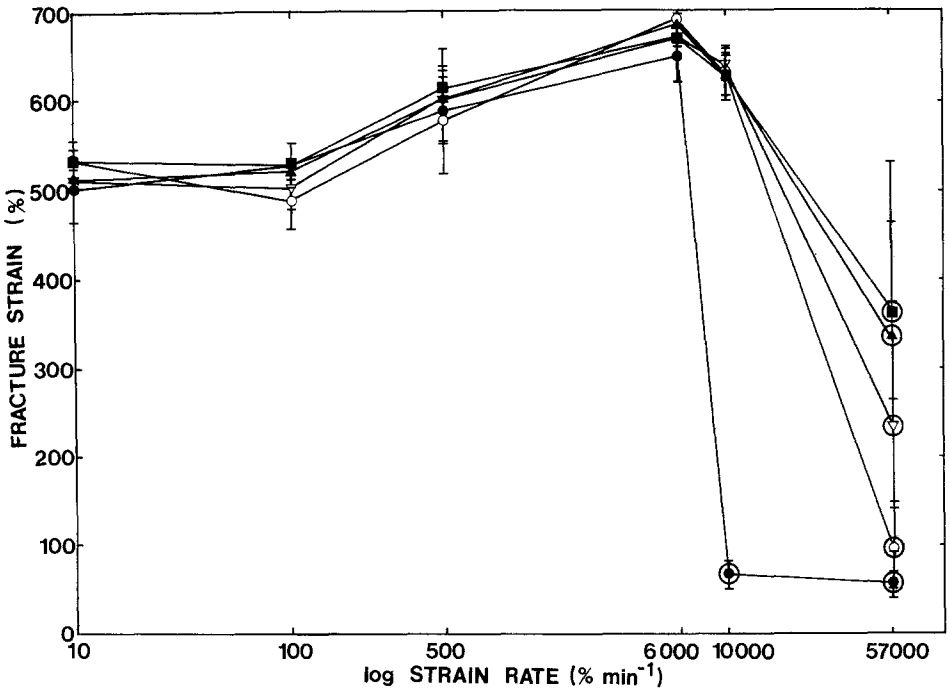

Figure 11 Average fracture strain against strain rate for all the Cleartuf 1006 PET–olefin compositions, ● PET, ■ PET–LLDPE, ▲ PET–HDPE, ▽ PET–PP, ○ PET–TPX.

3.2.2. Irreversible deformation behaviour

All specimens deformed by neck formation and subsequent propagation at all strain rates. The necks formed in the Vituf 1001A and Cleartuf 7207 PET tensile specimens were translucent in appearance at all strain rates except 6000% min^{-1}, where the necked material formed from Cleartuf 7207 PET was substantially whitened and opaque. All the LLDPE blends exhibited necked regions which were white and opaque at all strain rates.

The average yield stress of Cleartuf 7207 PET and its blends as a function of strain rate was similar to that obtained for the Vituf 1001A–LLDPE blends. A decrease in yield stress by approximately 10 to 12% was observed with the addition of 5% LLDPE. Blending 10% LLDPE with Cleartuf 7207 PET resulted in a yield stress drop of approximately 20 to 22%. The yield stress increased linearly with strain rate for all compositions.

As previously observed, specimens fractured during work hardening at low strain rates, but at higher strain rates the specimens fractured during the cold drawing process. Plots of fracture strain against strain rate for the LLDPE blends are shown in Figs 16 and 17. Fracture which occurred during cold drawing is represented by the circled points. A comparison of the fracture behaviour for the three polyesters can be made by examining Figs 11, 16 and 17. Similar behaviour was observed for strain rates less than 500% min^{-1} and greater than 10000% min^{-1}. Significant

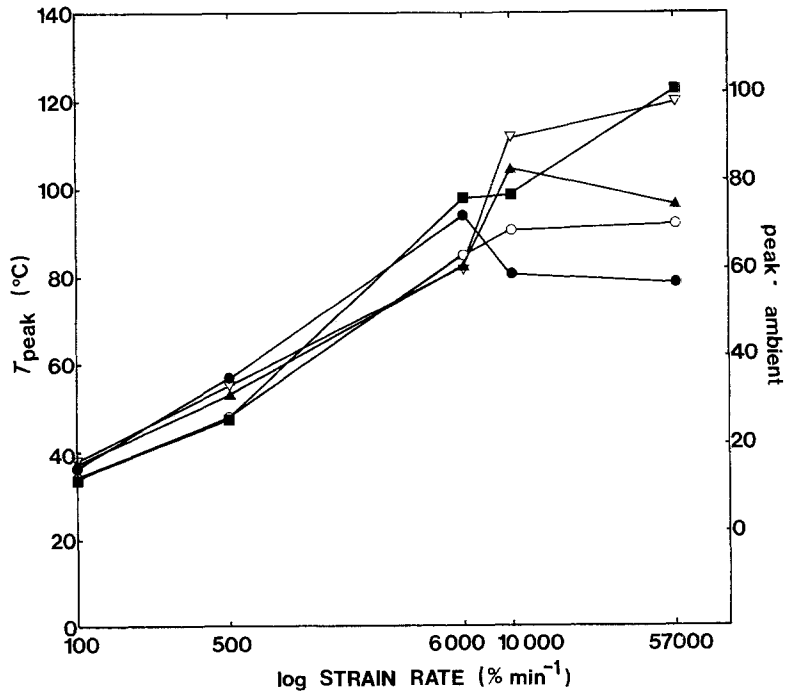

Figure 12 The peak temperature, T_p, of the propagating neck front and the difference between the peak temperature and the ambient temperature, T_a, $(T_p - T_a)$, as a function of strain rate for Cleartuf 1006 PET and the PET–olefin blends, ● PET, ■ PET–LLDPE, ▲ PET–HDPE, ▽ PET–PP, ○ PET–TPX.

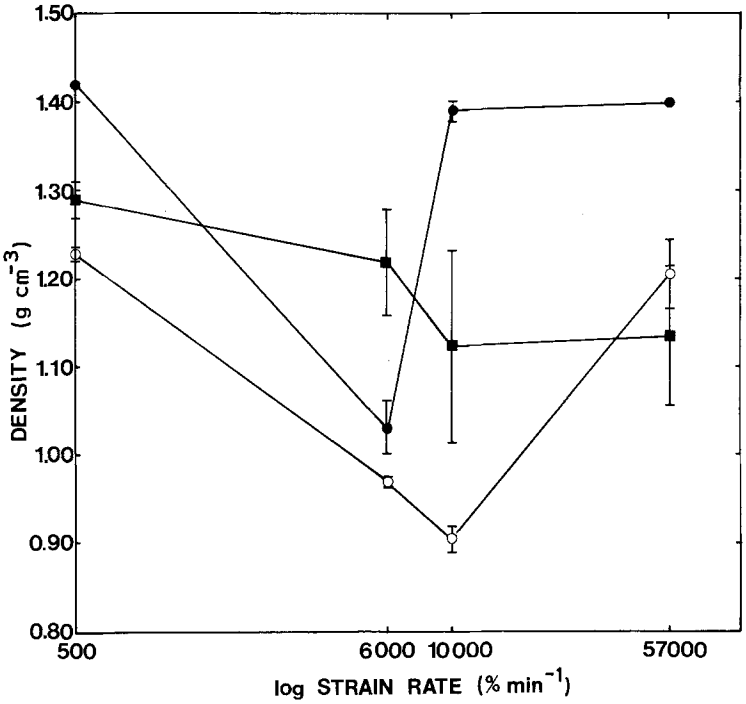

Figure 13 Densities of undeformed specimens and deformed tensile samples of Cleartuf 1006 PET, PET–LLDPE and PET–TPX evaluated as a function of strain rate. Undeformed density (g cm^{-3}) ● PET = 1.39 ± 0.010, ■ PET–LLDPE = 1.360 ± 0.010, ○ PET–TPX = 1.369 ± 0.002.

differences in fracture behaviour were observed in the strain rate regime of the transition from work hardening fracture to cold drawing fracture. However, no essential differences were noted when any of the resins were blended with 3% LLDPE.

Similar fracture behaviour was observed with changes in composition from 1 to 5% LLDPE. The transition in strain at fracture for 10% LLDPE blended with Cleartuf 7207 occurred at a lower strain rate than for the 1 to 5% LLDPE blends. For example, the transition in fracture strain is complete for the 10% LLDPE blends but only midway for the 1 to 5% blends at the highest strain rate. However, the transition for the 10% LLDPE blend was shifted to a higher strain rate than for the homopolymer.

Both the peak temperature, T_p, and the difference between T_p and the ambient temperature, T_a, $(T_p - T_a)$ as a function of strain rate for the Cleartuf 7207 blends are shown in Fig. 18. The temperature at the propagating neck increased steadily with strain rate. However, at the highest strain rates, 10 000 and 57 000% min^{-1}, the values of T_p for PET levelled at approximately the T_g of PET, while average T_p values for the PET–olefin blends as high as 135° C were observed.

4. Discussion

4.1. Crystallization behaviour

The olefin particles do not act as nucleating agents during PET crystallization from the melt since they have essentially no effect on the degree of supercooling, but cause a decreased rate of crystallization and an increase in crystallite or spherulite size and size distribution. A decrease in the crystallization growth rate has been reported for a number of blend systems containing a low concentration of the second component [21–23]. It is thought that expenditure of energy in rejection and/or occlusion of the olefin particles by the growing spherulitic front results in the

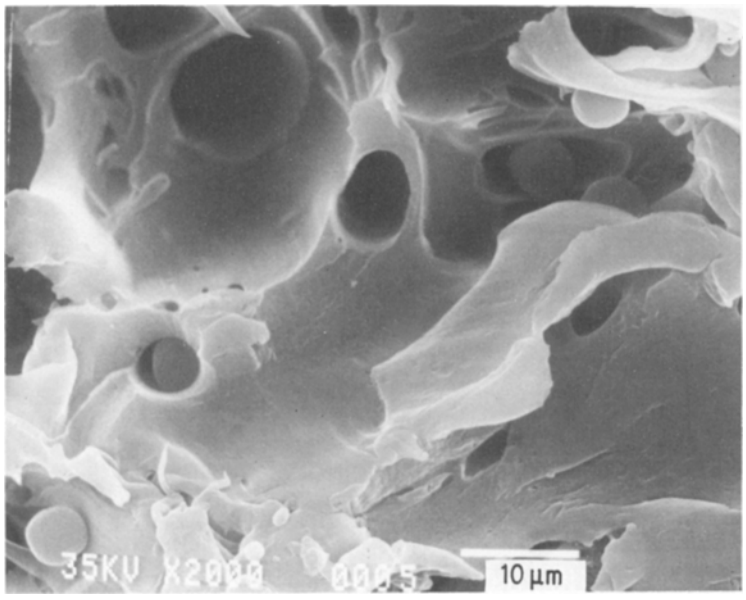

Figure 14 SEM micrograph of the freeze fractured surface of the necked portion of a PET–TPX tensile specimen drawn to fracture at 500% min^{-1}.

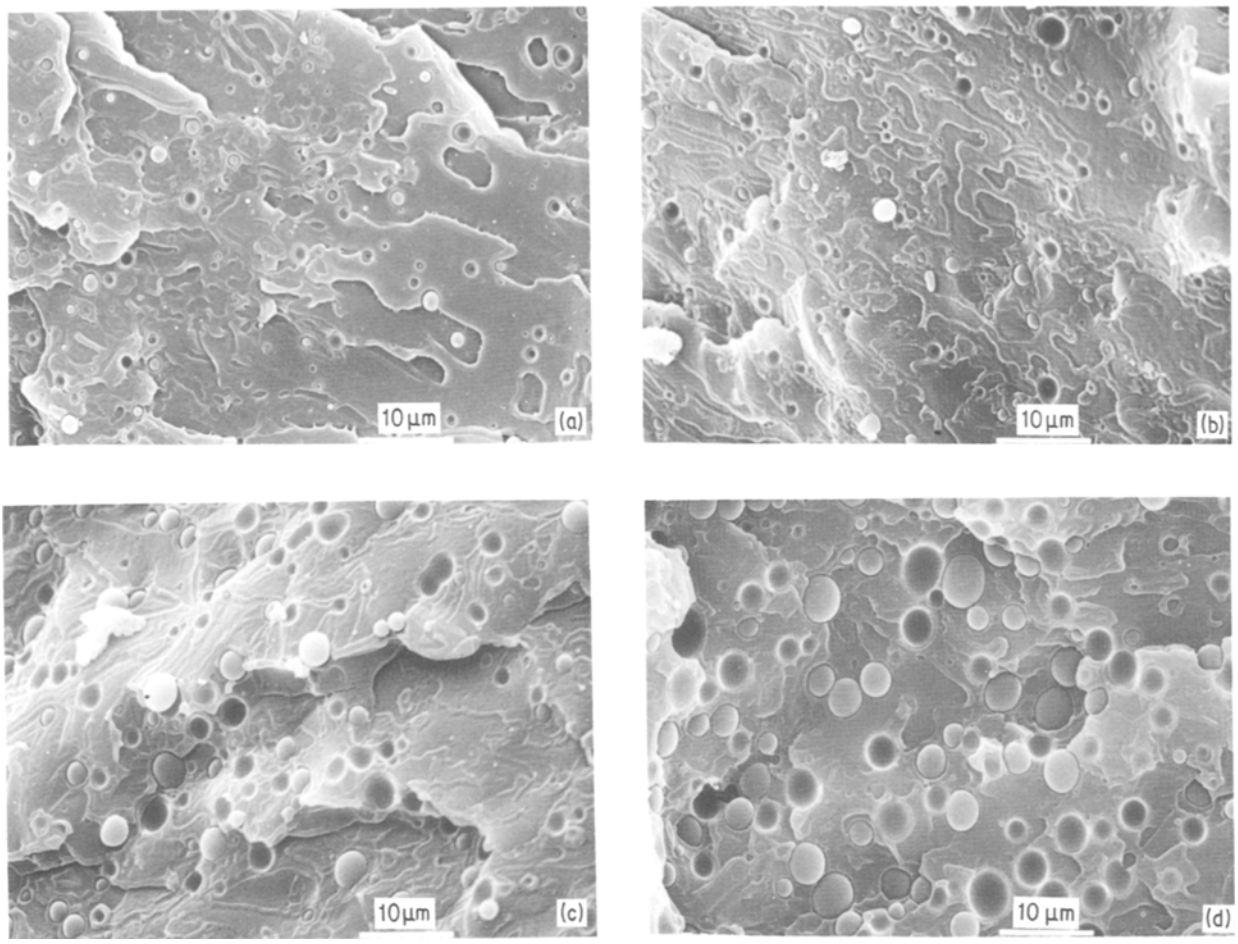

Figure 15 SEM micrographs of the freeze fractured surfaces for Cleartuf 7207 PET blended with 1, 3, 5 and 10% LLDPE.

observed depression of the crystallization growth rate [24–26].

In PET–LLDPE and PET–HDPE blends, the olefin appears to nucleate cold crystallization of glassy PET. Since both LLDPE and HDPE, but not PP or TPX, melt before the onset of cold crystallization, it is suggested that the volume expansion associated with olefin melting creates stress concentrations which induce PET crystallization. The effect was more pronounced with LLDPE than HDPE and is attributed to the lower melting temperature of the former.

4.2. Heat generation during cold drawing

A transition from an isothermal to an adiabatic condition with increased strain rate has been reported for PET [27–29]. It is generally accepted that yielding

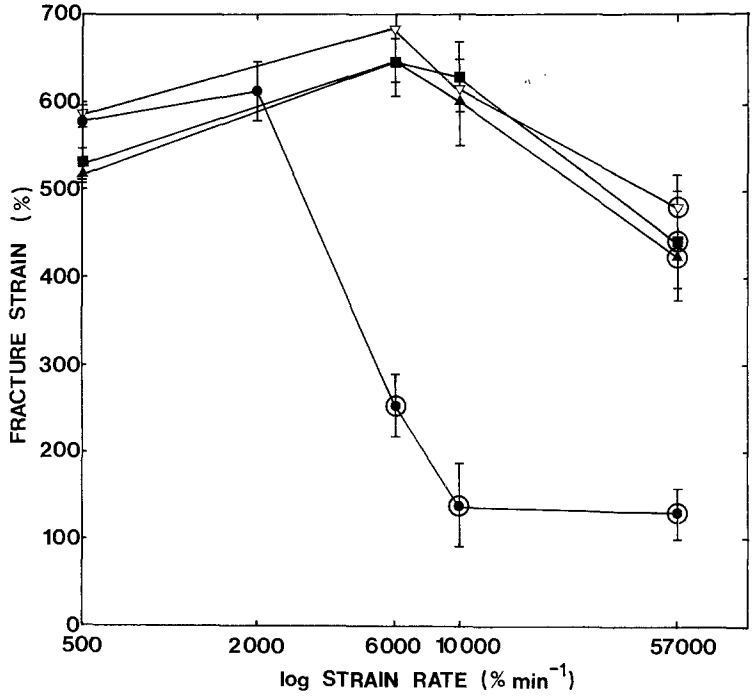

Figure 16 Average fracture strain as a function of strain rate for Vituf 1001A PET and the PET–LLDPE blend compositions. Fracture which occurred during cold drawing is represented by the circled points, ● PET, ▽ PET–1% LLDPE, ■ PET–3% LLDPE, ▲ PET–5% LLDPE.

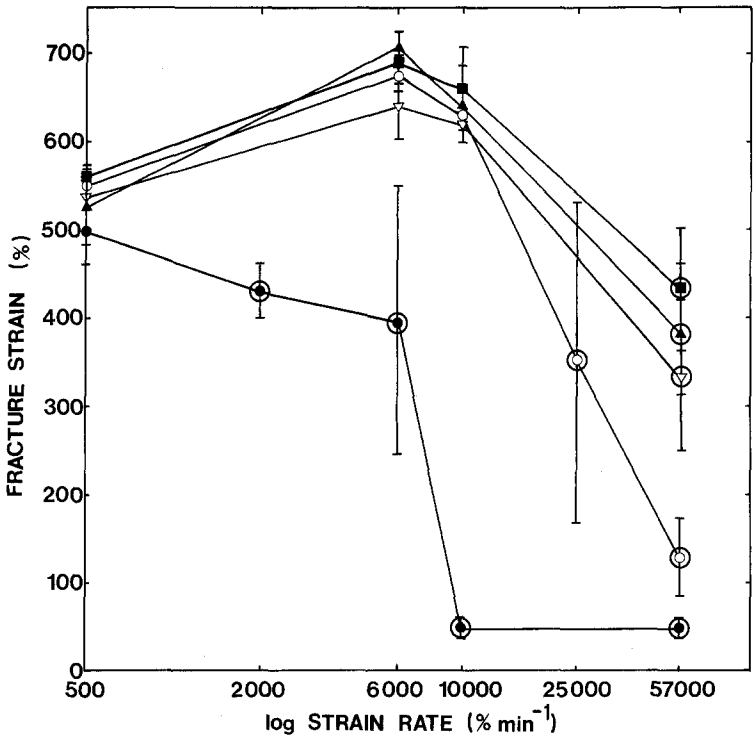

Figure 17 Average fracture strain as a function of strain rate for Cleartuf 7207 PET and the PET–LLDPE blend compositions. Fracture which occurred during cold drawing is represented by the circled points, ● PET, ▽ PET–1% LLDPE, ■ PET–3% LLDPE, ▲ PET–5% LLDPE, ○ PET–10% LLDPE.

occurs under isothermal conditions, and adiabatic heating is associated with the cold drawing process [29–31]. This can be shown by examining the plots of yield stress and draw stress against strain rate. The yield stress measured for PET increased with strain rate, while the drop in draw stress, which corresponded with the transition in fracture behaviour, suggests that adiabatic heating affects the mechanical behaviour.

The amount of mechanical work done on a specimen and the associated heat generated during the cold drawing process has been quantified for several polymers [32, 33]. The quantity of mechanical work in J g^{-1} for PET and the blends was evaluated from the area under the draw portion of the stress–strain curve according to the expression

$$\textit{mechanical work} = Fge \qquad (1)$$

where F is the drawing force in kg, g is the gravitational constant, and e is the elongation per unit mass of drawn material in m kg^{-1}. The amount of measurable heat in J g^{-1} was calculated from the following

$$\textit{measurable heat} = C_p(T_p - T_a) \qquad (2)$$

where C_p is the specifc heat (1125 J kg^{-1} K^{-1}), T_p is the peak temperature in °C and T_a is the ambient temperature in °C.

Both the mechanical work done on the specimen and the heat generated during cold drawing were analysed specifically for Cleartuf 1006 PET and the PET–LLDPE blend. The mechanical work and the measurable heat calculated at various strain rates are shown in Table I. The difference between the mechanical work and measurable heat is the heat dissipated to the surroundings during cold drawing. The ratio of measurable heat to mechanical work is shown in Fig. 19 as a function of strain rate. At low strain rates, the

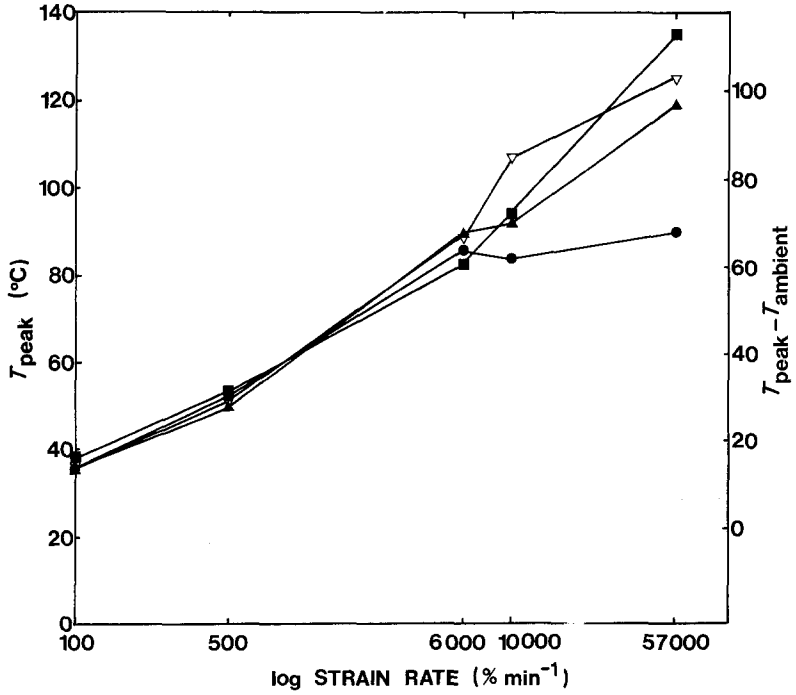

Figure 18 The peak temperature, T_p, of the propagating neck front and the difference between the peak temperature and the ambient temperature, T_a, $(T_p - T_a)$, as a function of strain rate for Cleartuf 7207 PET–LLDPE blends, ● PET, ▽ PET–1% LLDPE, ■ PET–3% LLDPE, ▲ PET–5% LLDPE.

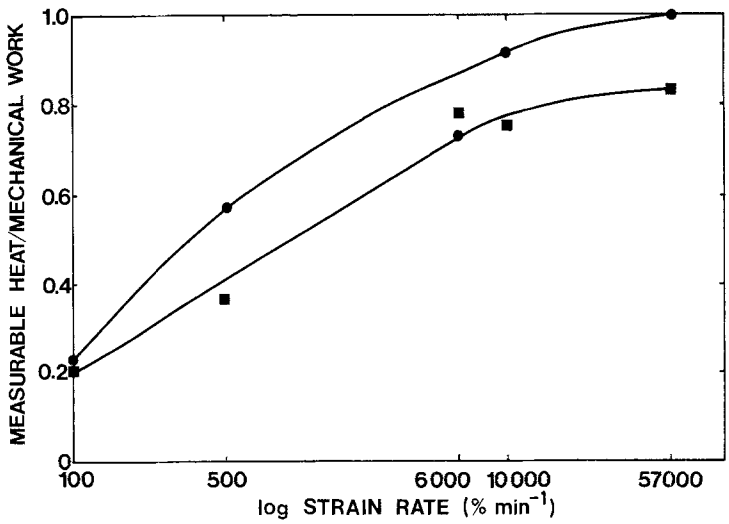

Figure 19 The ratio of measurable heat : mechanical work as a function of strain rate, ● PET, ■ PET–LLDPE.

cold drawing is intrinsically isothermal. At high strain rates, essentially adiabatic conditions prevail for PET. However, only 80% of the work appears as measurable heat for the PET–LLDPE blend due to the higher temperatures reached during cold drawing.

The heat generated during cold drawing is comprised of melting of the olefin particles, strain induced crystallization, and plastic deformation. Only the temperature rise during deformation at 57 000% min^{-1} is sufficient to melt the LLDPE particles. The small amount of heat evolved, 2 J g^{-1} of blend, contributes insignificantly to the total heat.

Heat evolved during strain induced crystallization can be estimated from the heat of fusion which ranged from approximately 35 to 43 J g^{-1} for specimens strained at rates of 100 and 10 000% min^{-1}, respectively. Thus, more than half the mechanical work for PET and approximately a third for the PET–LLDPE blend can be associated with strain induced crystallization.

The heat generated from plastic deformation can be approximated by a fracture mechanics anaysis of fracture energy [34]. For the PET–olefin blends, the fracture energy is comprised of the reversible work of adhesion and the irreversible plastic work or viscoelastic dissipation. The work of adhesion calculated for 3% polyethylene particles of 1 μm diameter in a PET matrix is an insignificant 0.8 J g^{-1}.

The major contribution to the fracture energy is the plastic deformation. Values reported for the irreversible plastic work in ductile polymers such as poly(methyl methacrylate) are about 200 J m^{-2} [34]. With this value, the fracture energy calculated for the blend system with 3% particles 1 μm in diameter is greater than 200 J g^{-1}. Clearly, the remaining portion of the mechanical work done on the specimen can be accounted for by plastic deformation. The difference in the mechanical work between PET and the PET–LLDPE blend is accounted for in plastic deformation.

TABLE I Values of the mechanical work and measurable heat for Cleartuf 1006 and PET–LLDPE determined at strain rates of 100 to 57 000% min^{-1}

Composition	Strain rate (% min^{-1})	Mechanical work (J g^{-1})	Measurable heat (J g^{-1})
PET	100	58.1 ± 1.5	13.5 ± 4.8
	500	70.9 ± 5.1	40.5 ± 4.8
	6000	106.4 ± 3.4	77.6 ± 3.4
	10 000	69.6 ± 15.4	63.0 ± 2.5
	57 000	62.0 ± 16.7	63.0 ± 8.0
PET–LLDPE	100	58.2 ± 1.6	12.4 ± 0.0
	500	75.3 ± 1.7	27.0 ± 1.6
	6000	103.8 ± 8.7	82.1 ± 0.0
	10 000	111.8 ± 15.0	83.3 ± 6.6
	57 000	132.1 ± 24.9	110.3 ± 4.5

4.3. Toughening mechanism in PET blends

A transition from work hardening fracture to cold drawing fracture for PET and the blends is observed with strain rate. This transition does not affect yielding and is not a ductile to brittle transition but a ductile to ductile transition. The transition is contingent on the stability of the neck during cold drawing and is shifted to higher strain rates for the PET–olefin blends. The stability and strength of the propagating neck depends on strain induced crystallization and orientation. It is proposed that the rates of crystallization and orientation during cold drawing with the subsequent stabilization of the propagating neck are greater for the blends than for PET.

Faster rates of crystallization and orientation of PET in the blends can be attributed to the local stress fields surrounding the olefin particles. It is well known that particles distributed in a polymer matrix act as stress concentrators. In polycarbonate, the stress concentrations around the polyethylene particles act as sites for shear initiation during deformation [16]. In PET, the deformation mechanism involves shear processes, so the embedded particles act to enhance the local shear stresses. Thus, the enhanced drawability and toughness of PET in the blends are controlled by the kinetics of strain induced crystallization and orientation of the propagating neck.

At low strain rates where the cold drawing process is essentially isothermal, both PET and the PET–olefin blends exhibit similar mechanical behaviour. As the strain rate increases and the cold drawing process becomes more adiabatic, the temperature in the deformation zone also increases. For PET, when the temperature reaches the T_g, a transition in the mechanical properties is observed. It is proposed that the rates of strain induced crystallization and orientation are insufficient for stabilization of the propagating neck, and

consequently, the mechanical behaviour is controlled by the rubbery phase. A decrease in both draw stress and fracture strain results.

At high strain rates, the temperatures measured for the PET–olefin blends are substantially above T_g. However, the mechanical properties are not controlled by a rubbery phase but by an oriented crystalline phase. This stabilization of the propagating neck at temperatures above T_g can be attributed to faster rates of crystallization and orientation in the blend compositions. This is probably due to strain induced crystallization and orientation at the particles.

In the PET–olefin blends, toughening is attributed to enhanced shear processes at the olefin particles which subsequently allow increased rates of crystallization and orientation to occur at high strain rates. The enhanced shear processes do not appear to be sensitive to olefin particle size in the range of 0.1 to 3 μm in diameter. However, larger particles display a decreased effectiveness in toughening PET. This is probably due to the enlarged region of enhanced stress surrounding the particles which can lead to crack formation.

Strain induced crystallization of PET is greater with LLDPE particles than with the other olefins. This may be a result of higher stress concentrations created by volume expansions upon melting of the particles during deformation. Although the temperature rise during deformation is sufficient to melt the LLDPE particles, the small amount of heat evolved does not contribute to the energy balance.

5. Conclusions

This study of the rate dependent deformation behaviour of PET and its blends leads to the following conclusions.

1. A sharp transition from work hardening fracture to cold drawing fracture was observed for PET and its blends with strain rate. This transition is dependent on the stability of the propagating neck and is shifted to higher strain rates for the blends.

2. Both PET and its blends exhibit similar mechanical behaviour at low strain rates where the cold drawing process is essentially isothermal. As the strain rate increases and the cold drawing process becomes more adiabatic, the associated temperature increases, in some cases, 50° C above T_g. For PET, the rate of strain induced crystallization and orientation is insufficient for stabilization of the propagating neck, and consequently, the mechanical properties are controlled by the rubbery phase.

3. The enhanced drawability of PET blended with low concentrations (1 to 10%) of olefin is attributed to the increased rates of crystallization and orientation. This increase in kinetics is attributed to strain induced crystallization and orientation at the stress fields surrounding the olefin particles. The strain induced effect is magnified with LLDPE particles as a result of volume expansion from melting of the particles during deformation.

Acknowledgement

The authors thank Dr B. Pengilly and Dr R. Smith for numerous stimulating discussions. The generous financial support of The Goodyear Tyre and Rubber Company and the National Science Foundation (grant ISI 8116103) through their co-sponsorship of the Center for Applied Polymer Research is gratefully acknowledged.

References

1. C. B. BUCKNALL and R. R. SMITH, *Polymer* **6** (1965) 37.
2. C. B. BUCKNALL, in "Toughened Plastics" (Applied Science, London, 1977) pp. 137–80.
3. R. P. KAMBOUR, *J. Polym. Sci. Macromol. Rev.* **7** (1973) 1.
4. S. G. TURLEY and H. KESKKULA, *Polymer* **21** (1980) 466.
5. A. M. DONALD and E. J. KRAMER, *J. Appl. Polym. Sci.* **27** (1982) 3729.
6. J. D. MOORE, *Polymer* **12** (1971) 478.
7. J. SILBERBERG and C. D. HAN, *J. Appl. Polym. Sci.* **22** (1978) 599.
8. B. Z. JANG, D. R. UHLMANN and J. BB. VANDERSANDE, *ANTEC, Soc. Plast. Eng. Conf.* (1984) 549.
9. M. R. GRANCIO, *Polym. Eng. Sci.* **12** (1972) 213.
10. A. M. DONALD and E. J. KRAMER, *J. Mater. Sci.* **17** (1982) 1765.
11. R. P. PETRICH, *Polym. Eng. Sci.* **13** (1973) 248.
12. H. BREUER, F. HAAF and J. STABENOW, *J. Macromol. Sci. Phys.* **B14** (1977) 387.
13. A. SIEGMANN, L. K. ENGLISH, E. BAER and A. HILTNER, *Polym. Eng. Sci.* **24** (1984) 877.
14. S. WU, *J. Polym. Sci. Polym. Phys. Ed.* **21** (1983) 699.
15. S. Y. HOBBS, R. C. BOPP and V. H. WATKINS, *Polym. Eng. Sci.* **23** (1983) 380.
16. M. A. MAXWELL and A. F. YEE, *ibid.* **21** (1981) 205.
17. A. F. YEE, *J. Mater. Sci.* **12** (1977) 757.
18. L. J. BROUTMAN and S. SAHU, *Mater. Sci. Eng.* **8** (1971) 98.
19. J. LEIDNER and R. T. WOODHAMS, *J. Appl. Polym. Sci.* **18** (1974) 1639.
20. S. K. BROWN, *Brit. Polym. J.* **12** (1980) 24.
21. A. GALESKI, Z. BARTCZAK and M. PRACELLA, *Polym.* **25** (1984) 1323.
22. A. K. GUPTA and S. N. PURWAR, *J. Appl. Polym. Sci.* **29** (1984) 1598.
23. A. ESCALA and R. STEIN, in "Multiphase Polymers" edited by S. L. Cooper and G. M. Estes, Advances in Chemistry Series 176 (American Chemical Society, Washington DC, 1979) p. 1053.
24. E. MARTUSCELLI, C. SILVESTRE and G. C. ABATE, *Polymer* **23** (1982) 229.
25. E. MARTUSCELLI, C. SILVESTRE and L. BIANCHI, *ibid.* **24** (1983) 1458.
26. Z. BARTCZAK, A. GALESKI, E. MARTUSCELLI and C. N. R. ARCO FELIZE, *Polym. Eng. Sci.* **24** (1984) 1155.
27. I. MARSHALL and A. B. THOMPSON, *Proc. R. Soc.* **A221** (1954) 541.
28. G. P. ANDRIANOVA, A. S. KECKEKYAN and V. A. KARGIN, *J. Polym. Sci. A-2* **9** (1971) 1919.
29. S. W. ALLISON and I. M. WARD, *Brit. J. Appl. Phys.* **18** (1967) 1151.
30. P. I. VINCENT, *Polymer* **1** (1960) 7.
31. I. M. WARD, in "Mechanical Properties of Solid Polymers" (Wiley Interscience, New York, 1983) Ch. 11.
32. A. CROSS and R. N. HAWARD, *J. Polym. Sci. Polym. Phys. Ed.* **11** (1973) 2423.
33. J. W. MAHER, R. N. HAWARD and J. N. HAY, *ibid.* **18** (1980) 2169.
34. S. WU, "Polymer Interface and Adhesion" (Marcel Dekker, New York, 1982) Ch. 10.

Received 11 July
and accepted 12 August 1985